Energy Conversion and Management 300 (2024) 117879

Contents lists available at ScienceDirect

Energy Conversion and Management

journal homepage: www.elsevier.com/locate/enconman

Machine learning-driven optimization of Ni-based catalysts for catalytic steam reforming of biomass tar

Nantao Wang [a,1], Hongyuan He [a,1], Yaolin Wang [a,1], Bin Xu [b], Jonathan Harding [a], Xiuli Yin [b], Xin Tu [a,*]

[a] Department of Electrical Engineering and Electronics, University of Liverpool, Liverpool L69 3GJ, UK
[b] CAS Key Laboratory of Renewable Energy, Guangdong Provincial Key Laboratory of New and Renewable Energy Research and Development, Guangzhou Institute of Energy Conversion, Chinese Academy of Sciences, Guangzhou 510640, China

ARTICLE INFO

Keywords:
Machine learning
Biomass gasification
Tar reforming
Syngas
Toluene
Catalytic reforming

ABSTRACT

Biomass gasification is a promising process for producing syngas, which is widely used in various industrial processes. However, the presence of tar in syngas poses a significant challenge to biomass gasification due to the difficulties in its removal and potential downstream issues, such as clogging, slagging, and corrosion. Extensive efforts have been made to address this challenge through catalytic tar removal using various catalysts, generating a vast amount of experimental data. Processing this large dataset and gaining new insights into process optimization requires the development of efficient data analysis methods. In this study, a comprehensive database was built, encompassing a total of 584 data points and 14 input parameters collected from literature published between 2005 and 2020. Machine learning algorithms were then trained using this dataset to predict and optimize the catalytic steam reforming of biomass tar. The predicted results were found to agree well with the experimental data. The results show that the reaction temperature is the most important process parameter, with the highest relative importance of 0.24, followed by the support (0.16), additive (0.12), nickel (Ni) loading (0.08), and calcination temperature (0.07), among the 14 input parameters. This work has proposed optimal ranges for the reaction temperature (600–700 °C), Ni loading (5–15 wt%), and calcination temperature (500–650 °C). Furthermore, it was found that a larger specific surface area and higher Ni dispersion are two critical factors for selecting additives and supports. This study provides insights into key parameters for optimizing the catalytic steam reforming of biomass tar, enabling enhanced efficiency and effectiveness in biomass gasification processes.

1. Introduction

Nowadays, fossil fuels play a predominant role in meeting most of the world's energy needs, leading to global warming, the greenhouse effect, and other environmental issues [1]. Biomass is a renewable and nearly carbon–neutral energy source, making it promising for sustainable energy production when compared to fossil fuels [2–4]. In recent years, significant efforts have been devoted to biomass gasification for the production of syngas, which can be further converted into platform chemicals and valuable fuels via Fischer-Tropsch synthesis (FTS) [5,6]. Unfortunately, the formation of tar has impeded the commercialization of biomass gasification, as it can cause clogging, slagging, and corrosion issues in downstream equipment and processes [7–9]. Tar typically presents as a dense, dark brown to black, highly viscous liquid characterized by its complex composition. It encompasses a diverse array of chemical components, ranging from single-ring to multiple-ring aromatic compounds, to other oxygen-containing hydrocarbons and intricate polycyclic hydrocarbons [10,11]. Among these constituents, toluene and naphthalene emerge as the predominant components,

Abbreviations: ANN, Artificial neural networks; AUC, Area under each receiver operating characteristic curve; DT, Decision tree; FTS, Fischer-Tropsch synthesis; GBCT, Gradient boosting classifier tree; LR, Logistic regression; ML, Machine learning; PCA, Principal component analysis; ROC, Receiver operating characteristic; RI, Relative importance; RMSE, Root mean squared error; RF, Random forest; SVM, Support vector machine; S/C, Steam-to-carbon; WGS, Water-gas shift; XGB, Extreme gradient boosting classifier tree.

* Corresponding author.
E-mail address: xin.tu@liverpool.ac.uk (X. Tu).
[1] These authors have the same contribution to this study.

https://doi.org/10.1016/j.enconman.2023.117879
Received 3 September 2023; Received in revised form 5 November 2023; Accepted 11 November 2023
Available online 9 December 2023

Nomenclature

R^2	Coefficient of determination
Symbols	
Al	Aluminum
Co	Cobalt
Ce	Cerium
Cu	Copper
Ca	Calcium
Fe	Iron
K	Potassium
Mn	Manganese
Mo	Molybdenum
Mg	Magnesium
Ni	Nickel
Pd	Palladium
Pt	Platinum
Ru	Ruthenium
Sr	Strontium
Si	Silicon
Zr	Zirconium

collectively constituting approximately 75% of the tar's composition. Notably, toluene stands out as the most abundant compound within the composition of tar [12].

Various technologies have been explored to address the issue of tar removal, including mechanical separation [11], thermal cracking [13], catalytic reforming [14], and plasma-based reforming [15]. Among these technologies, catalytic reforming has emerged as a promising approach due to its capability to generate syngas with an adjustable hydrogen (H_2) content, reduce energy waste compared to mechanical separation, and operate at lower temperatures than thermal cracking [5,16,17]. In particular, toluene has often been selected as the model compound in the catalytic reforming of tar as it represents one of the primary tar components generated during high-temperature biomass gasification processes [18–22].

Nickel (Ni)-based catalysts are widely used in the catalytic reforming of tar due to their affordability, high catalytic activity, and ability to break carbon–carbon bonds effectively [23]. Extensive studies have been conducted to investigate the catalytic steam reforming of toluene using Ni-supported catalysts. This includes varying the Ni loading (5 to 20 wt%), using different supports (Al_2O_3, ZrO_2, TiO_2, CeO_2, MgO, etc.) and adding certain elements (Co, Ce, Fe, Mn, Mo, etc.) [24–28]. In addition to catalyst modifications, extensive research has also focused on exploring various operating parameters, including reaction temperature, reaction time and steam-to-carbon (S/C) ratio [28–34]. However, the abundance of experimental data poses challenges in effectively utilizing it due to the presence of numerous parameters and their complex interactions. To overcome this issue, data analysis tools such as machine learning (ML) algorithms can be employed to comprehensively analyze the entire database and uncover important trends and connections that may have been overlooked by researchers.

Machine learning is a powerful tool that mimics human learning and can uncover complex patterns, trends, and correlations among multiple variables [35,36]. Several studies [37] have used pioneering algorithms to investigate biomass conversion, yielding promising results, as shown in Table S1. Tang et al. applied random forest (RF) and support vector machine (SVM) algorithms to predict the yield and composition of pyrolytic gas under different pyrolysis conditions and biomass types [38]. Leng et al. employed random forest algorithms to study the production of nitrogen heterocycles in bio-oil during hydrothermal liquefaction of high-moisture biomass, revealing the significance of nitrogen content, nitrogen-to-carbon ratio, and protein in the production of nitrogen heterocycles [39]. Smith et al. investigated the water–gas shift (WGS) reaction using artificial neural networks (ANN) and principal component analysis (PCA), highlighting that reaction temperature is the most important parameter affecting the WGS reaction [40]. Shafizadeh et al. [41] conducted a comprehensive study focusing on the co-pyrolysis of biomass and coal, employing a diverse array of machine learning algorithms, including support vector regression, ANN, RF regression, and gradient boosting regression. Of these methods, the gradient boosting regression exhibited remarkable accuracy, showcasing a coefficient of determination (R^2) exceeding 0.96. The investigation found that the operating temperature and the biomass blending ratio were the most significant parameters in the co-pyrolysis of biomass and coal. Additionally, the study extended its contributions to practical implications by formulating optimization recommendations. These recommendations encompassed the selection of operating temperature, biomass blending ratios, and heating rate to enhance the efficacy of the co-pyrolysis process, shedding valuable light on this critical area of research.

For the catalytic steam reforming of toluene, Shafizadeh et al. [12] blazed a trail by employing ensemble machine learning techniques to forecast toluene conversion and syngas composition. Their predictions hinged upon an amalgamation of catalysts' characteristics and operating parameters, yielding favorable outcomes. Nevertheless, it is noteworthy that their investigation predominantly relies on the characterization data of catalysts, with a limited exploration into pivotal parameters within the catalyst preparation process, such as metal loading, and the selection of additives and supports, which merit further research. Yahya et al. [42] conducted a study that integrates experimental findings with the ANN algorithm to investigate the relationship between hydrogen (H_2) production and various operational parameters in the context of catalytic steam reforming of toluene. Their investigation sought to optimize critical parameters, including reaction temperature, feed gas flow rate, catalyst mass, S/C ratio, etc. Notably, their research revealed that reaction temperature exerted the most pronounced influence on H_2 production within the process. However, the practical application of the optimized operational parameters remains constrained, given that their analysis exclusively centered on a specific catalyst, specifically Ni-Co supported modified-activated carbon.

Hence, this investigation initiated its exploration with Ni-based catalysts and established a comprehensive database encompassing all pertinent parameters associated with the catalytic steam reforming of toluene. This database comprised 14 key parameters, which were categorized into three distinct groups: catalyst, preparation, and operation. Machine learning algorithms were subsequently employed to analyze these parameters for process optimization. Initially, the RF algorithm was utilized to obtain the relative significance of each parameter. Subsequently, the ANN algorithm was employed to elucidate the interactions among these influential parameters. Finally, optimization strategies for enhancing the catalytic steam reforming of toluene were proposed. These strategies encompassed insights into the judicious selection of suitable supports and additives, as well as the identification of optimal operational conditions. These proposed strategies were empirically validated through experimental trials employing γ-Al_2O_3 as support.

2. Method

The method employed in the study can be subdivided into three primary phases, delineated as database construction, machine learning, and optimization, as depicted in Fig. 1. Initially, an exhaustive literature review was conducted, and 14 parameters pertinent to the process and the physicochemical properties of the selected catalysts were extracted from peer-reviewed publications. Subsequently, the extracted dataset was utilized to train a suite of machine learning algorithms, comprising five classification algorithms: logistic regression (LR) classifier, decision tree (DT), RF classifier, extreme gradient boosting classifier tree (XGB),

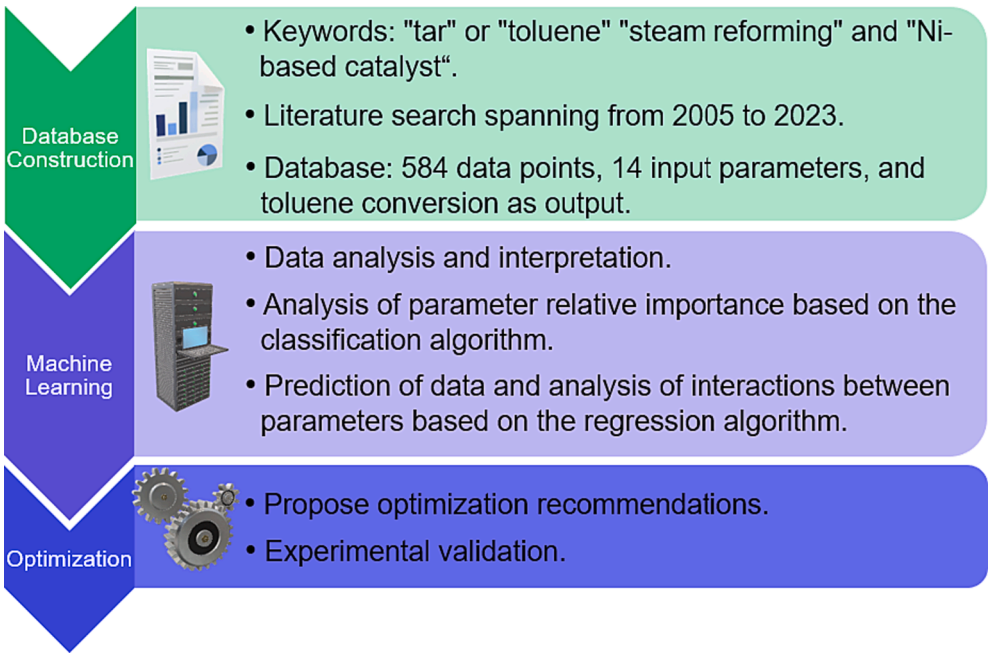

Fig. 1. The research method used in this study.

and gradient boosting classifier tree (GBCT), alongside a regression algorithm: the ANN algorithm. Finally, optimization strategies are proposed for enhancing the catalytic steam reforming of toluene based on meticulous analysis of the relative importance and interactions among these parameters, followed by validation through experiments.

2.1. Database construction and pre-processing

A database of 584 data points was manually collected from relevant literature published between 2005 and 2020. The details of the database are presented in the supplementary material (Table S2). To convert non-numerical parameters, such as support, additive, preparation method, into valid input formats (vectors), a one-hot encoding method was used. For instance, the support was represented by 1 in the category it belongs to, and other supports were represented by 0. Within this database, it is important to note that not all catalysts employed in the studies under consideration incorporated additives. Consequently, in cases where no additives were utilized, data is absent in the cells designated for "additive type" and "additive content." To address this situation, a pragmatic solution has been implemented by unifying the "additive content" variable into the one-hot encoding schema linked to "additive". Instead of employing binary values (0 or 1) within the respective column, this study utilizes the exact "additive content" value. In the meantime, numerical parameters, such as Ni loading, reaction temperature, and calcination temperature, were labelled with their actual values. Utilizing the one-hot encoding method facilitates maintaining data consistency without incorporating extraneous details. After one-hot encoding, each data set was represented as a 72-dimensional vector, while the toluene conversion was represented as a target 1-dimensional vector, as shown in Table S3.

The encoded data was then transformed to have unit variance using a standard scaler. This reduced the effect of distributional inconsistencies due to the different units of measurement. The standard scaler was calculated based on equation (1).

$$z = \frac{x - \mu}{s} \tag{1}$$

where z is the transformed vector, x is the original one-hot vector, μ is the mean value, and s represents the standard deviation.

2.2. Classification algorithms

Five classification algorithms were first trained to identify the most important parameters for high toluene conversion, including the LR classifier, DT classifier, RF classifier, XGB, and GBCT. LR is a parametric model that utilizes a logistic function, while other algorithms are non-parametric models that rely on a tree-like structure to make predictions. DT uses one tree for classification, while RF, XGBoost, and GBCT classifiers use multiple trees. To ensure a fair comparison, an effort was made to maintain consistency in the parameters, with the maximum depth of the four tree algorithms being fine-tuned within a reasonable range (as specified in Table S4). Decision trees resemble flowcharts and can be used to predict the effectiveness of catalysts based on their chemical and physical characteristics. They make decisions based on simplistic principles that are determined by the tree's structure. In the study, the internal nodes of the decision trees corresponded to feature judgements, each branch to the decision or result of the judgement, and each leaf node to the classification label or type. Toluene conversion was employed as an indicator for the catalytic steam reforming of toluene, with a classification standard set for toluene conversion above or below 90%. This resulted in 30% of the data being classified as high and 70% being classified as low, striking a balance between ML and chemical intuition in terms of the categorical distribution of the data. The hyper-parameters were chosen based on their impact on prediction performance and were limited to a narrow range to minimize the effect on the prediction accuracy due to the non-overlapping hyper-parameters of different algorithms, as shown in Table S4. To mitigate the risk of overfitting, 5-fold cross-validation was employed to evaluate the classification performance of the trained algorithms on a specific randomly selected training set. The entire dataset was divided into five randomly selected subsets, also known as "slices". During each validation iteration, four slices were used as the training set, and the remaining fifth slice served as the validation set. This process was repeated five times, with each slice taking turns as the validation set. The prediction accuracy was evaluated using equation (2).

$$\text{accuracy}(y, \hat{y}) = \frac{1}{n_{\text{samples}}} \times \sum_{i=0}^{n_{\text{samples}}-1} 1 \ (\hat{y}_i = y_i) \tag{2}$$

where $\widehat{y_i}$ is the predicted value of the i-th sample and y_i represents the experimental value.

In this study, the performance of various algorithms was evaluated not only based on accuracy but also using receiver operating characteristic (ROC) curves. ROC curves are widely used to visualize, organize, and select classification algorithms based on their performance in radio, medicine, and biology, lately machine learning has also become popular in other fields [43,44]. To construct a ROC curve, a threshold of determination was specified, allowing the calculation of coordinate points from the experimental values and predicted values of all samples (high or low). These points were then connected by a continuous line, forming the ROC curve within the interval of 0 to 1. The ROC space is divided into upper left and lower right areas by a diagonal line running from (0, 0) to (1, 1). Points above the diagonal line represent excellent classification (better than random classification), while those below the line represent poor classification (inferior to random classification). Furthermore, the area under each ROC curve (AUC) was calculated to quantify the classification performance. A higher AUC indicates a better classification algorithm. Unlike overall accuracy, which considers only one cutpoint, the ROC curve considers all cutpoints and plots, making it more robust, particularly in cases of sample imbalance. Since the developed dataset has an uneven distribution of positive and negative samples, adopting ROC as a complementary performance metric for model evaluation helps address the issue of sample imbalance and provides a more comprehensive evaluation of the algorithms' capabilities.

The relative importance (RI) of each parameter was determined by calculating the impurity gain (Gini importance), which measured the overall decrease in impurity caused by each parameter, as indicated in equation (3). The Gini importance is a statistical metric that quantifies the relevance of each parameter in machine learning. It measures the extent to which a feature contributes to the model's ability to discriminate between different classes or outcomes. In the context of this study, Gini importance helps to identify which parameters have the most significant influence on the classification of toluene conversion, which is essential for optimizing the catalytic steam reforming of toluene.

$$G_i = \sum_k \left(1 - p_{i,k}\right) p_{i,k} \tag{3}$$

where $p_{i,k}$ represents the ratio of all training data classified as class k in the i-th node. For the non-tree-based algorithm LR, the relative importance is determined using the coefficients of the features. All RIs are normalized to ensure that their sum equals 1.

2.3. Artificial neural network algorithm

The ANN, being a well-established and mature algorithm is widely employed for predictive purposes in the domain of biomass utilization [40–42]. After the most significant features were identified from the classification models, an ANN was employed to train a regression algorithm for predicting the exact values of toluene conversion. Derived from the comprehension of relative importance acquired through classification algorithms, the ANN can be more effectively optimized, overfitting can be circumvented, and the accuracy of the algorithm can be enhanced. Then, a well-trained ANN algorithm was employed to perform a grid search over the relatively more important features, such as reaction temperature, additive, support, calcination temperature, and Ni loading to investigate their interaction. An ANN algorithm was preferred over other algorithms due to its ability to achieve a greater goodness of fit while avoiding overfitting by balancing the network's breadth and depth. In this study, a fully linked, feed-forward topology with five layers, including input and output layers, was selected for the ANN architecture. Each layer consisted of a linear function with m nodes and a bias node b, as shown in equation (4). The output of the node was subsequently processed by the Sigmoid activation function, as defined in equation (5), to achieve non-linear fitting. Considering that the data is sampled from various sources and tends to be discrete, the Layer Normalization technique (https://arxiv.org/abs/1607.06450) was incorporated to mitigate the overfitting of the algorithm.

$$y = w_1x_1 + w_2x_2 + \cdots + w_mx_m + b \tag{4}$$

$$\text{Sigmoid}_{(y)} = \frac{1}{1 + e^{-y}} \tag{5}$$

where y is the output value of a node, w_m is the weight of the m-th input node value, and b represents the bias value.

The entire database was divided randomly into five folds, and each fold was chosen once as test data, resulting in ten distinct data selections. For each data selection, 5 individual ANNs were trained, and the training process was terminated based on the test accuracy inflection point. To avoid over-fitting, the final predicted value of the ANN was averaged across the 5 individual ANNs, functioning as a hybrid model. Meanwhile, the performance of the ANN algorithm was evaluated using the R^2 and root mean squared error (RMSE), as defined in equations (6) and (7), respectively. A method for Stochastic Optimization (Adam) with a learning rate γ of 0.0005 was adopted as the optimizer.

$$R^2(y, \widehat{y}) = 1 - \frac{\sum_{i=1}^{n}(y_i - \widehat{y_i})^2}{\sum_{i=1}^{n}(y_i - \bar{y})^2} \tag{6}$$

$$\text{RMSE} = \sqrt{\frac{1}{n}\sum_{i=1}^{n}(y_i - \widehat{y_i})^2} \tag{7}$$

where n is the number of the test dataset, equivalent to the number of ANN; y_i, $\widehat{y_i}$, and $\bar{y}$ are the experimental value, the corresponding predicted value, and the mean value of the n experimental values, respectively.

3. Results and discussion

3.1. Description of the database

In this study, a comprehensive database was built, encompassing a total of 584 data points and 14 input parameters collected from literature published between 2005 and 2020, as presented in Table S2. 14 major parameters are identified as key experimental indicators and categorized into three groups: catalyst, preparation, and operation. The catalyst group includes Ni loading, additive, additive content, and support. The preparation section is responsible for the preparation method, calcination temperature, calcination time, reduction temperature, and reduction time. Meanwhile, the group of operating parameters consists of the reaction temperature, reaction time, S/C ratio, feed gas, and feed gas flow rate. The toluene conversion was chosen as the assessment index.

The database is briefly summarized in Table S5, and Fig. 2 presents the statistical distribution of the numerical parameters. As shown in Fig. 2a, the Ni loading ranges from 1 to 40 wt% and is mostly distributed between 5 and 12 wt%. The additive content ranges from 0.08 to 29.8 wt % (mostly within 0.9–2.9 wt%), which is lower than the Ni loading. Fig. 2b displays the range of parameters for catalyst preparation, including calcination temperature (350 to 1300 °C, mainly within 600–800 °C), reduction temperature (150 to 950 °C, mainly within 650–800 °C), calcination time (1 to 6 h, mainly within 2–4 h), and reduction time (0.5 to 8 h, mainly within 1–2.5 h). These parameters represent typical conditions for catalyst preparation. Fig. 2c shows that the reaction temperature, reaction time, feed gas flow rate, and S/C ratio are commonly within the ranges of 300–900 °C, 0.25–24 h, 30–1500 mL/min, and 0.4–6.5, respectively.

Simultaneously, Figure S1 presents the Pearson correlation coefficient matrix between toluene conversion and the input numerical

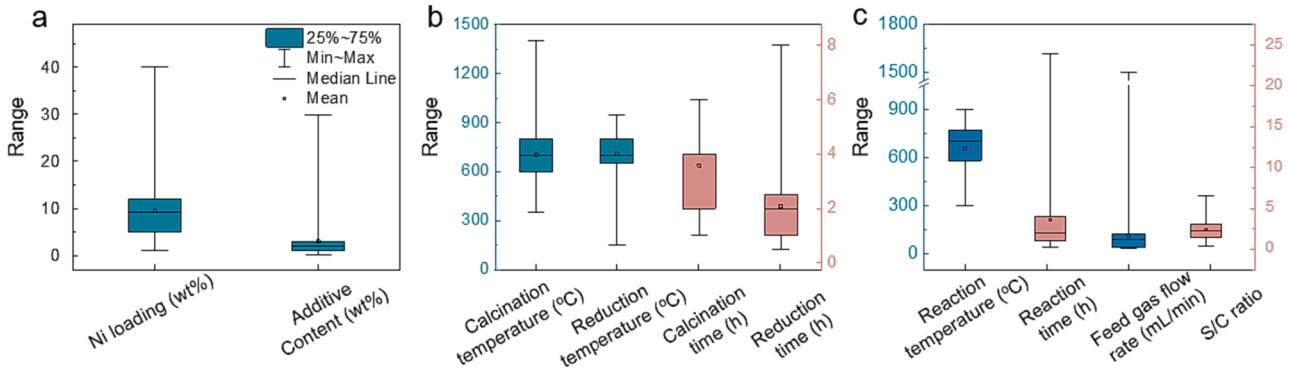

Fig. 2. The statistical distribution of different parameters in the category of (a) catalyst, (b) preparation, and (c) operation.

parameters. Notably, the reaction temperature exhibits a positive correlation with toluene conversion, with a correlation coefficient of 0.18. This correlation can be attributed to the highly endothermic nature of catalytic steam reforming of toluene [11]. An elevated reaction temperature can facilitate the steam reforming and thermal cracking reactions of toluene to a certain extent. Furthermore, Ni loading demonstrates a positive correlation with toluene conversion, supported by a correlation coefficient of 0.16, since increasing Ni loading could provide sufficient active sites for the reaction [13]. On the other hand, reaction time is inversely correlated with toluene conversion, potentially caused by catalyst deactivation during prolonged reaction times [45].

In addition to the numerical parameters, the database also includes non-numerical parameters, such as additive, support, preparation method, and feed gas. Additive types vary depending on the types of metals, such as noble metals (Pd, Pt, Sr, etc.), non-noble metals (Fe, Cu, etc.), alkali metal (K), alkali earth metals (Mg, Ca, etc.), and bimetals (Ce-Mg, Ru-Mn, etc.). The support contains natural ores (hydrotalcite, dolomite, olivine, mayenite, etc.), widely used supports (HZSM-5, γ-Al_2O_3, SBA-15, CaO, TiO_2, SiO_2, MgO, etc.), and some unconventional supports (biochar, coal ash, graphitic mesoporous carbon, etc.). Wet impregnation is the most commonly used method for catalyst preparation, followed by co-impregnation and co-precipitation. Nitrogen (N_2) and argon (Ar) are the most frequently used feed gases in the catalytic steam reforming of toluene.

3.2. Selection of classification algorithms

Firstly, an appropriate classification algorithm was chosen from five typical tree-based algorithms based on their classification performance to determine the relative importance of each parameter. As shown in Fig. 3a, the accuracy of different algorithms ranges from 0.83 to 0.99, with RF and GBCT achieving the highest accuracy at 0.99. Since RF and GBCT had the same accuracy, ROC curves were then employed to further evaluate the classification performance of different tree-based algorithms. As depicted in Fig. 3b, the diagonal line from (0, 0) to (1, 1) separated the ROC space into upper left and lower right regions, with points above the line indicating excellent classification (better than random classification) and points below the line representing poor classification (inferior to random classification). Meanwhile, the AUC is calculated to quantify classification performance, with a higher AUC indicating greater accuracy. After comparing the ROC curve and AUC value, RF was selected with an accuracy of 0.99 and an AUC value of 0.92. In the meantime, RF exhibits a reduced propensity to inaccurately register true positives in comparison to other algorithms, thus showcasing a more conservative stance, as shown in the confusion matrix in Fig. S2. Such a judgement criterion is also pivotal when discerning relative importance, ensuring that influential features genuinely exert a pronounced effect on conversion.

3.3. Relative importance analysis

The relative importance of different parameters was determined by calculating impurity gain (Gini importance) based on the RF shown in Fig. 4a. The reaction temperature has the highest relative importance (0.24), followed by the support (0.16), additive (0.12), Ni loading (0.08), and calcination temperature (0.07), among others. Previous research by Yahya and coworkers also found that the reaction temperature was the most significant parameter for the catalytic steam reforming of toluene over Ni-Co supported modified-activated carbon, owing to the endothermic nature of the steam reforming process [42]. The higher relative importance of reaction temperature could be attributed to the highly endothermic nature of the process and the instability of the catalyst induced by temperature [46]. On the one hand,

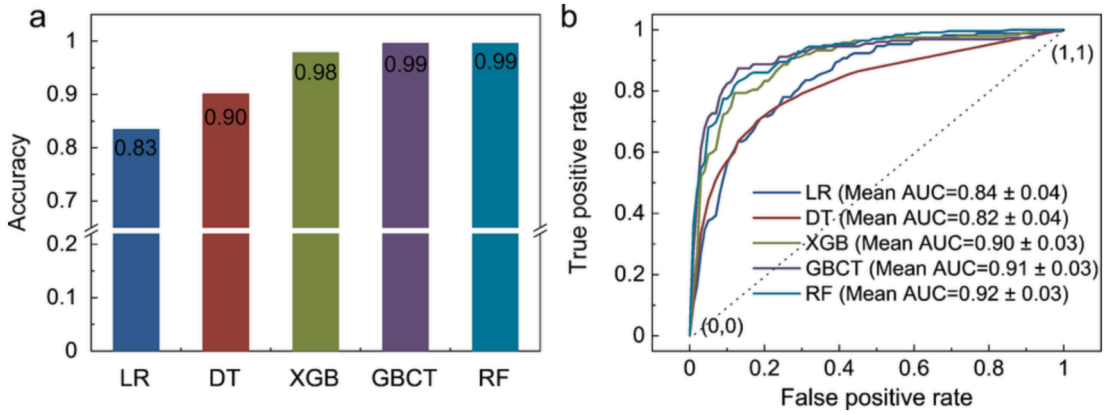

Fig. 3. (a) The accuracy and (b) the mean ROC curves of different classification algorithms.

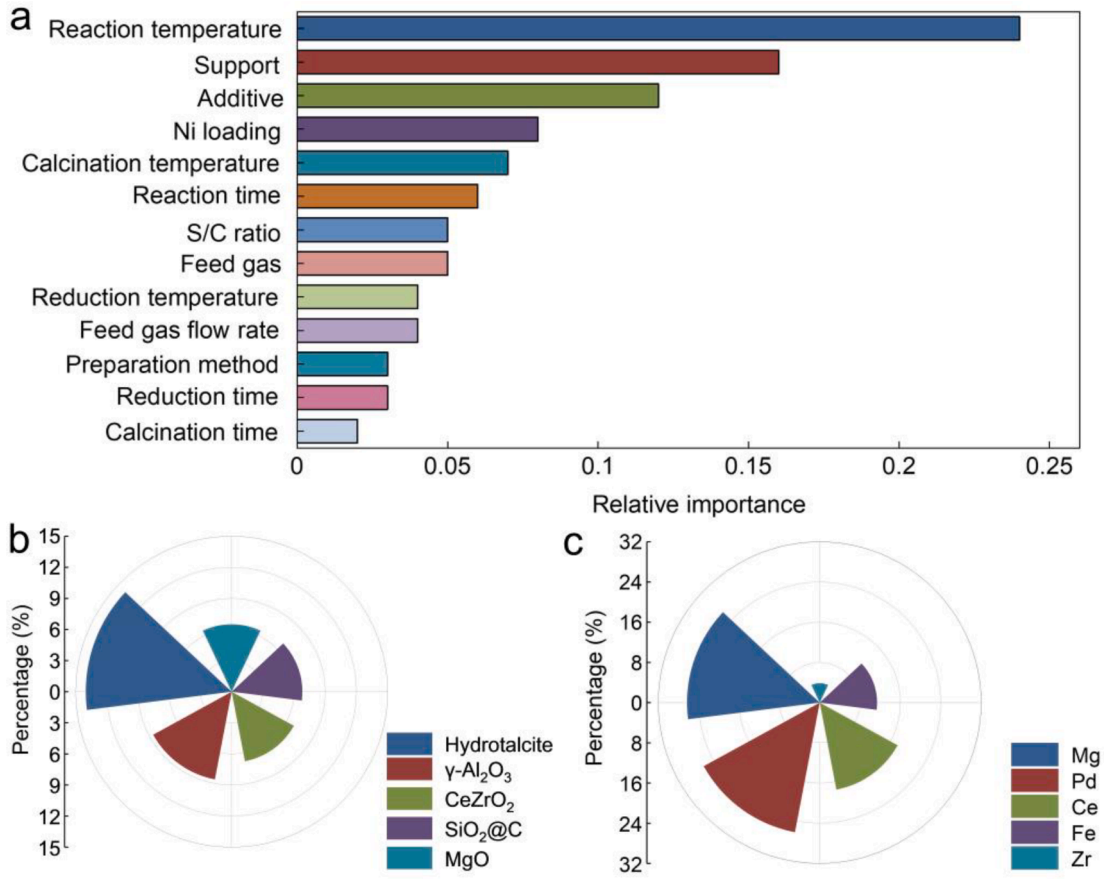

Fig. 4. (a) The relative importance of each parameter, and the percentage of different (b) supports and (c) additives in the category of support and additive, respectively.

the activation energy of the reaction highly relies on temperature. On the other hand, catalysts will suffer deactivation due to carbon deposition and sintering at higher temperatures [47]. The deposited carbon encases the active metal particles, making it impossible for reactants to reach the active site, while sintering leads to the clumping of metal particles, reducing the available active metal surface, and deteriorating the catalytic activity [46,48].

The support is the second most important parameter in the study due to its unique properties, such as specific surface area, thermal stability, mechanical strength, oxygen storage and release capacity, and resistance to carbon deposition, etc. [49]. Choosing a proper support could not only improve the catalytic activity but also enhance the stability of the catalyst. For instance, Ni-loaded carbon-coated mesoporous silica ($Ni/SiO_2@C$) exhibited a higher toluene conversion of 99.9% with excellent stability for at least 46 h at 550 °C, which was attributed to the enhanced metal-support interaction with graphitic carbon layers protecting the highly dispersed Ni nanoparticles that were embedded into the silica wall of mesoporous channels [45]. As shown in Fig. 4b, hydrotalcite has the highest relative importance in the category of support, followed by γ-Al_2O_3, $CeZrO_2$, $SiO_2@C$, etc. When compared with these supports, hydrotalcite shows a relatively higher specific surface area (151 m^2/g) and the biggest average pore diameter (22.1 nm), as depicted in Table S7, which improves Ni dispersion and exposes more active sites on the support. Zhou et al. [50] found that Fe-promoted Ni/hydrotalcite catalysts showed higher catalytic activity and stability, reaching almost 100% toluene conversion at 400 °C for 3 h. Furthermore, the model simulation shows that Fe-promoted Ni/hydrotalcite has a good adsorption affinity with toluene, which increases toluene accessibility to the active sites [50].

The additive ranks third with a relative importance of 0.12. Incorporating additive metals is a common approach to modify Ni-based catalysts as Ni is prone to coke formation reactions, leading to catalyst deactivation [49]. By interacting with Ni to generate an alloy, the additive could modify surface properties and improve catalytic performance in terms of activity and stability. Lu et al. [28] investigated the effects of different additives (Co, Ce, Fe, Mn, and Mo) on catalytic steam reforming of toluene over Ni-based catalysts and discovered that Mo-modified Ni-based catalysts exhibited the highest catalytic activity, with a toluene conversion of 92.6%, owing to the formation of a Mo-Ni alloy. Meanwhile, the formation of the Mo_2C structure improved the carbon resistance of the catalyst [28]. As shown in Fig. 4c, Mg has a greater relative importance in the category of additive, and the research confirmed that the addition of Mg contributed to improving the resistance to carbon deposition of the catalysts through oxidization of deposited carbon with absorbed oxygen [51,52]. Moreover, various bimetal additives, such as Ru-Mn [47] and Ce-Mg [53] also enhanced the catalytic performance in terms of reactivity and stability. Besides the additive and support, Ni loading was another critical parameter. Optimal Ni loading could not only provide sufficient active sites but also prevent agglomeration caused by excessive loading [13].

In this study, calcination temperature is identified as the fifth most important parameter. Jumluck et al. previously discovered that the catalytic performance of the Ni/dolomite catalyst was significantly influenced by calcination temperature with toluene conversion dropping from 97.2 to 49.5% as the calcination temperature increased from 750 to 950 °C, at a reaction temperature of 730 °C. They found that the catalyst calcinated at 950 °C had a lower specific surface area (16.55 m^2/g) due to the support collapsing and metal sintering [24].

3.4. Validation of artificial neural network algorithm

An ANN algorithm was then used as a prediction algorithm to explore the interactions between the parameters. The fully linked, feed-forward topology (72–24–24–24-1) of the ANN enables a non-linear mapping between input and output data for prediction [54]. Experimental toluene conversion is plotted against predicted toluene conversion in Fig. 5a, which demonstrates the high accuracy of the adopted ANN algorithm in predicting toluene conversion, with an R^2 of 0.96. This R^2 is comparable to that of a previous study that used ANN for toluene conversion prediction with an R^2 of 0.95 [42]. Meanwhile, a detailed comparison between the experimental results and the predicted outcomes is presented in Fig. S3. For further exploration of the predictive ability of the trained ANN, a selection of recent published findings [14,20,48,55–57] (Table S6) not incorporated into the database was utilized as test data with the same ANN topology. While the model exhibits a degree of accuracy in predicting conversion rates, a discernible disparity between experimental and predicted values persists, as visually represented in Fig. 5b. The primary factor contributing to these prediction errors for novel experimental data might be the potential insufficiency of the training dataset. In machine learning, particularly for complex models, an ample volume of diverse data is imperative to facilitate the acquisition of meaningful patterns and relationships. Although the database comprises 584 data points, this quantity may still be deemed inadequate when correlated with the multitude of catalysts involved, potentially limiting the ability of the model to capture intricate data relationships.

3.5. Interaction between parameters and toluene conversion

In this section, the interaction between parameters with higher relative importance was examined by employing the well-trained ANN algorithm. As Mg and hydrotalcite were identified as the most prominent additive and support, respectively, they were selected initially for evaluating the interaction between toluene conversion, reaction temperature, calcination temperature, and Ni loading. Fig. 6 illustrates the contour maps of the interactions. Although different additives and supports were utilized, the interaction mechanisms of reaction temperature versus Ni loading (Fig. 6a and 6d), reaction temperature versus calcination temperature (Fig. 6b and 6e), and calcination temperature versus Ni loading (Fig. 6c and 6f) were found to be very similar.

As depicted in Fig. 6a and 6d, when the Ni loading is kept constant, the toluene conversion initially increases and then tends to remain constant as reaction temperature increases, which is attributed to the highly endothermic characteristics of the catalytic steam reforming of toluene [46]. Compared to Mg, the use of hydrotalcite as a support results in a higher toluene conversion at the same temperature due to improved Ni particle dispersion and toluene accessibility to the active sites [50]. In Fig. 6b and 6e, the toluene conversion initially increases and then decreases as the calcination temperature increases at a constant reaction temperature. This phenomenon is consistent with the findings reported by Jumluck et al., where they observed support collapse and metal sintered with increasing calcination temperature [24]. Moreover, this finding demonstrates that additives and supports respond differently to the calcination temperature. Specifically, Mg-promoted catalysts required a lower calcination temperature (around 600 °C) to achieve higher toluene conversion compared to hydrotalcite at the same reaction temperature and calcination temperature. Choosing an appropriate calcination temperature for different types of additives and supports is crucial for enhancing catalytic performance. Additionally, Ni loading exhibits a similar changing trend with calcination temperature when it comes to the conversion, as shown in Fig. 6c and 6f. It illuminates that a suitable amount of Ni loading could not only provide sufficient active sites but also inhibit agglomeration caused by excessive loading. Notably, Mg-promoted catalysts become sensitive as the calcination temperature approaches 600 °C, and the toluene conversion decreases significantly (Fig. 6c). In contrast, hydrotalcite-supported catalysts exhibit superior reaction temperature resistance, which is attributed to the improved thermal stability of the support [50].

Overall, the toluene conversion is found to depend on the interaction of multiple parameters, and appropriate ranges could be identified, such as 600–700 °C for reaction temperature, 5–15 wt% for Ni loading, and 500–650 °C for calcination temperature during catalyst preparation.

Meanwhile, these findings also enable one to offer insights for selecting additives and supports for the catalysts. Fig. 7 depicts the predicted conversion for the 5 most important additives and supports with different reaction temperatures, Ni loadings, and calcination temperatures. Table S7 summarizes the physicochemical properties of the corresponding catalysts, aiding in the comprehension of the effects of diverse additives and supports on the catalytic performance.

When using various additives (e.g., Mg, Pd, Ce, Fe, and Zr), the toluene conversion exhibits a similar trend with increasing reaction temperature, Ni loading, and calcination temperature, respectively (Fig. 7 a-c). The toluene conversion increases continuously as the reaction temperature and Ni loading increase. Pd-promoted catalysts show a lower catalytic performance among the additives. On the contrary, Mg, Ce, Fe, and Zr additives exhibit better toluene steam reforming performances, resulting from the promoted Ni dispersion and smaller Ni crystal size, as shown in Table S7 [50,52,57]. Proper additives could modify surface properties and improve the synergy between the metal and support, significantly enhancing catalytic performance in terms of activity and stability [58].

The results presented in Fig. 7 d-f demonstrate a similar changing trend in the toluene conversion using various supports when reaction

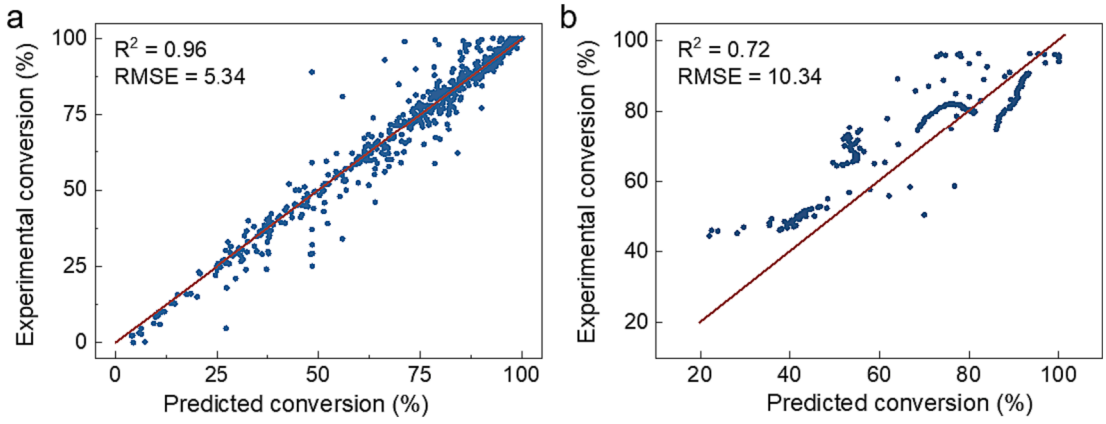

Fig. 5. The prediction performance of the ANN algorithm (purple line represented the best fitting: $y = x$) for (a) the current database and (b) data collected from newly published literature. (For interpretation of the references to colour in this figure legend, the reader is referred to the web version of this article.)

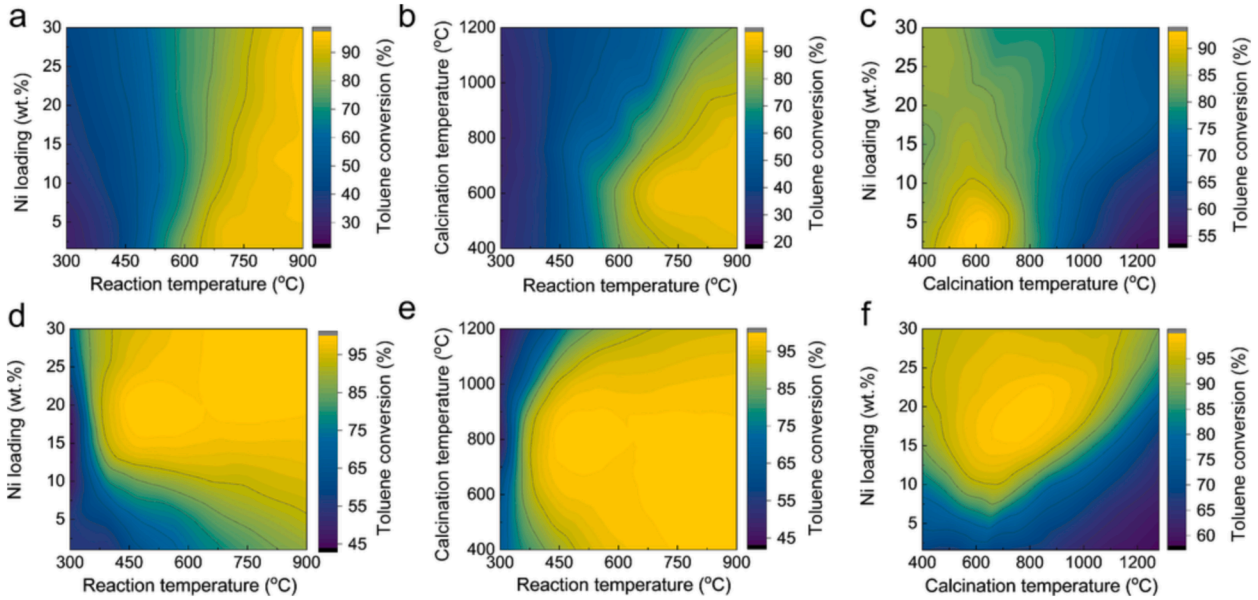

Fig. 6. The contour maps for the toluene conversion and temperature, calcination temperature, and Ni loading when using (a) (b) (c) Mg and (d) (e) (f) hydrotalcite as the additive and support, respectively.

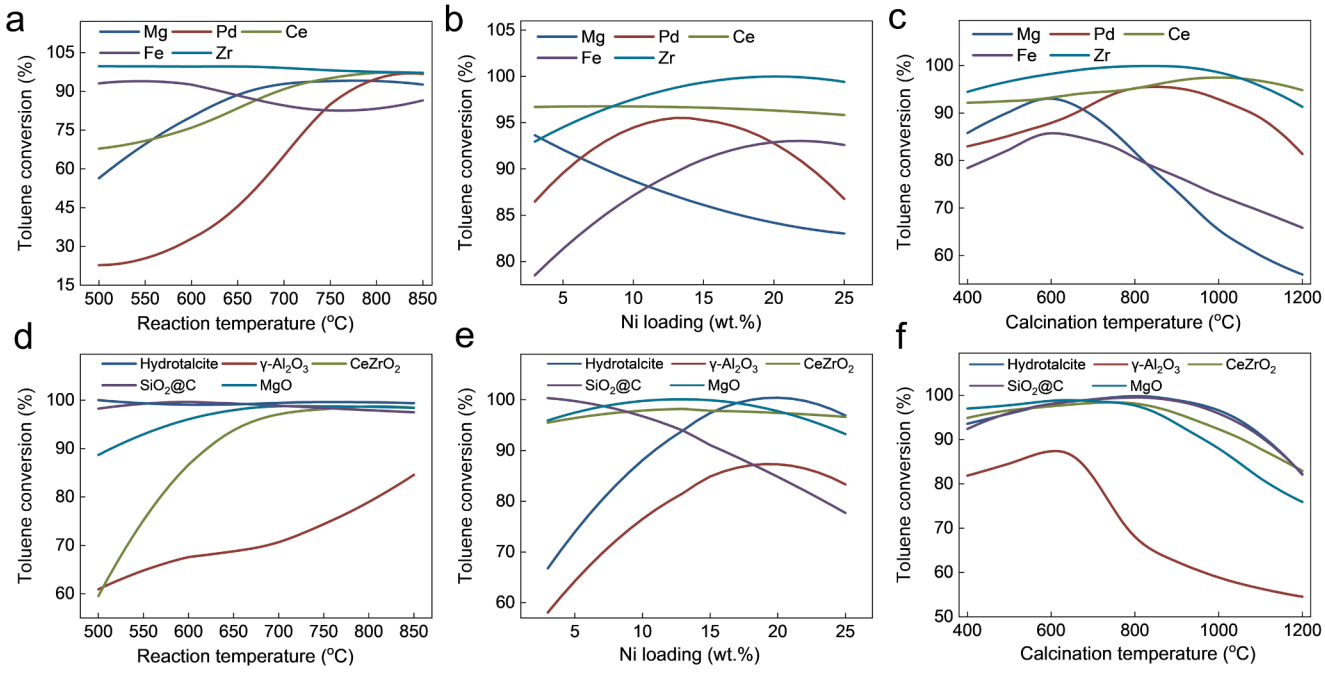

Fig. 7. The predicted toluene conversion over the top 5 additives and supports with (a) and (c) different temperatures, (b) and (e) Ni loading, and (c) and (f) calcination temperatures, respectively.

temperature, Ni loading, and calcination temperature increase. As depicted in Fig. 7d, the toluene conversion initially increases and tends to remain constant as reaction temperature increases, which is attributed to the highly endothermic characteristics of the catalytic steam reforming of toluene [46]. Meanwhile, various supports respond differently to Ni loading; the toluene conversion increases first and then declines when SiO_2@C and γ-Al_2O_3 supported catalysts are used. However, hydrotalcite achieves a higher toluene conversion when Ni loading reaches 20 wt%, which could be attributed to its higher specific surface area (150 m^2/g) [50]. SiO_2@C, MgO, $CeZrO_2$, and hydrotalcite supports exhibit better catalytic performances compared to γ-Al_2O_3 as the calcination temperature increases, which could be attributed to their superior thermal stability. Jumluck et al. reported that supports with poor thermal stability would collapse at higher calcination temperatures, resulting in a reduced specific surface area and catalyst deactivation [24]. These findings show that a higher specific surface area of the catalyst could not only bring sufficient active sites but also aid in Ni dispersion, resulting in a smaller Ni crystal size, which is beneficial for catalytic performance.

3.6. Process optimization

In this section, commercial γ-Al_2O_3 was selected as the support to optimize the catalytic steam reforming of toluene. In an effort to address

the issue of the relatively lower toluene conversion using Ni-loaded γ-Al_2O_3, a grid search was performed utilizing the ANN algorithm. The investigation revealed that the addition of Pt to Ni-loaded γ-Al_2O_3 catalysts could significantly enhance their toluene conversion capability, as depicted in Fig. 8a and 8d. Experiments were also conducted to validate the findings, and the detailed experimental sections were described in supporting information S7. Despite the existence of discrepancies in numerical values, it is evident that the ANN adeptly captures the overall trend in toluene conversion with varying temperatures, as shown in Fig. 8b. Moreover, it is worth noting that the ANN displays an exceptional predictive capacity, particularly in the case of 10Ni-1Pt/γ-Al_2O_3. The predicted values align closely with the corresponding experimental data. With the addition of 1 wt% Pt, the toluene conversion rises from 56.2 to 81.8% at 600 °C as compared to Ni loading alone. Furthermore, 10Ni-1Pt/ γ-Al_2O_3 achieves the highest toluene conversion of 97.8% at 700 °C. N_2 adsorption–desorption isotherm and X-ray powder diffraction (XRD) characterizations reveal that the specific surface area of the Pt-promoted catalyst reaches 139.3 m^2/g, while the Ni crystal size is reduced from 5.51 to 5.15 nm (Fig. 8c and S4). The higher specific surface area and smaller Ni crystal size might be responsible for the enhanced catalytic activity and stability of the Pt-promoted catalyst for the catalytic steam reforming of toluene.

4. Conclusions and prospects

In this study, a comprehensive database comprising 584 data points and 14 input parameters was constructed using literature published between 2005 and 2020. Well-trained machine learning algorithms were developed for the prediction and optimization of the catalytic steam reforming of toluene. The predicted results from algorithms are consistent with the experimental data, validating their effectiveness. The results reveal that the reaction temperature is the most influential parameter (0.24), followed by the support (0.16), additive (0.12), Ni loading (0.08), and calcination temperature (0.07). Appropriate ranges for influential parameters are identified. For instance, the recommended ranges were found to be 600–700 °C for reaction temperature, 5–15 wt% for Ni loading, and 500–650 °C for calcination temperature. These ranges are crucial for optimizing the catalytic process and achieving desirable toluene conversion rates. Moreover, this work also sheds light on the significance of selecting suitable supports and additives. The incorporation of appropriate supports and additives was found to enhance catalytic performance significantly. This was attributed to the provision of more active sites and the promotion of Ni dispersion, leading to improved activity and stability of the catalyst.

Although the study highlights the potential and benefits of well-trained ML algorithms for effective and accurate predictions and gaining deeper insights into the catalytic steam reforming of toluene as a tar model, it is essential to acknowledge the existing limitations that warrant attention in future research endeavors. In the study, the trained algorithms performed exceptionally well on the training database but failed to generalize to new, unseen data, resulting in discernible disparities between experimental and predicted values. The primary factor contributing to these prediction errors for novel experimental data might be the potential insufficiency of the training dataset. In machine learning, particularly for complex models, an ample volume of diverse data is imperative to facilitate the acquisition of meaningful patterns and relationships. Although the database comprises 584 data points, this quantity may still be deemed inadequate when correlated with the multitude of catalysts involved, potentially limiting the ability of the model to capture intricate data relationships.

In light of these observations, future research may prioritize enhancing the richness and breadth of the database. It is advisable to consider including additional input features, such as catalyst quality, morphology, thermogravimetric characteristics, pore distribution, acidity, elemental distribution, and other catalyst-specific attributes. It is essential to acknowledge the challenges associated with the collection and coding of such data. Furthermore, future research endeavors should explore the adoption of more complex and advanced models. This

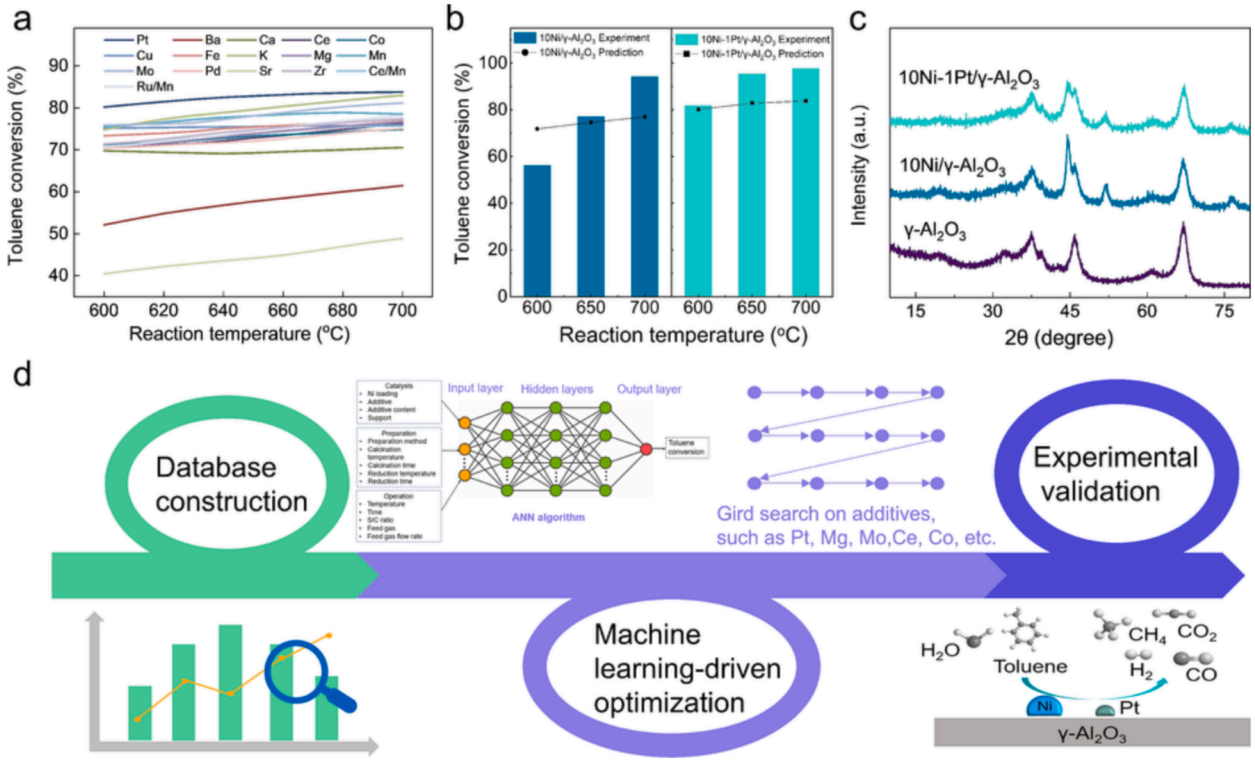

Fig. 8. (a) The predicted toluene conversion with different additives using γ-Al_2O_3 as support, (b) the experimental and predicted toluene conversion, (c) XRD patterns of the catalysts, and (d) the schematic diagram of machine learning-driven optimization and validation of catalytic steam reforming of toluene using γ-Al_2O_3 as support.

approach can potentially mitigate some of the limitations encountered by enhancing the capacity of the model to capture nuanced data relationships and yield more accurate predictions.

CRediT authorship contribution statement

Nantao Wang: Conceptualization, Methodology, Validation, Formal analysis, Investigation, Data curation, Writing – original draft, Visualization. **Hongyuan He:** Conceptualization, Methodology, Validation, Investigation, Data curation, Visualization. **Yaolin Wang:** Conceptualization, Methodology, Writing – review & editing. **Bin Xu:** Methodology, Validation, Formal analysis, Investigation. **Jonathan Harding:** Writing – review & editing. **Xiuli Yin:** Supervision, Resources, Funding acquisition. **Xin Tu:** Conceptualization, Resources, Writing – review & editing, Supervision, Project administration, Funding acquisition.

Declaration of Competing Interest

The authors declare that they have no known competing financial interests or personal relationships that could have appeared to influence the work reported in this paper.

Acknowledgement

This project has received the funding from the European Union's Horizon 2020 research and innovation programme under the Marie Sklodowska-Curie grant agreement (No. 823745). N. Wang thanks the joint scholarship programme co-funded by the University of Liverpool and the Chinese Scholarship Council.

Appendix A. Supplementary data

Supplementary data to this article can be found online at https://doi.org/10.1016/j.enconman.2023.117879.

References

[1] BP. Energy Outlook 2020 edition; 2020.
[2] Wang N, Zhan H, Zhuang X, Xu B, Yin X, Wang X, et al. Torrefaction of waste wood-based panels: More understanding from the combination of upgrading and denitrogenation properties. Fuel Process Technol 2020;206:106462. https://doi.org/10.1016/j.fuproc.2020.106462.
[3] Feng D, Zhang Y, Zhao Y, Sun S, Wu J, Tan H. Mechanism of in-situ dynamic catalysis and selective deactivation of H2O-activated biochar for biomass tar reforming. Fuel 2020;279:118450. https://doi.org/10.1016/j.fuel.2020.118450.
[4] Feng D, Zhao Y, Zhang Y, Xu H, Zhang L, Sun S. Catalytic mechanism of ion-exchanging alkali and alkaline earth metallic species on biochar reactivity during CO2/H2O gasification. Fuel 2018;212:523–32. https://doi.org/10.1016/j.fuel.2017.10.045.
[5] Xu B, Wang N, Xie J, Song Y, Huang Y, Yang W, et al. Removal of toluene as a biomass tar surrogate by combining catalysis with nonthermal plasma: understanding the processing stability of plasma catalysis. Catal Sci Technol 2020;10:6953–69. https://doi.org/10.1039/d0cy01211d.
[6] Miskolczi N, Gao N, Quan C. Pyrolysis-gasification of biomass and Municipal Plastic Waste using transition metal modified catalyst to investigate the effect of contaminants. J Energy Inst 2023;108:101233. https://doi.org/10.1016/j.joei.2023.101233.
[7] Mei D, Wang Y, Liu S, Alliati M, Yang H, Tu X. Plasma reforming of biomass gasification tars using mixed naphthalene and toluene as model compounds. Energ Conver Manage 2019;195:409–19. https://doi.org/10.1016/j.enconman.2019.05.002.
[8] Xu B, Xie J, Zhan H, Yin X, Wu C, Liu H. Removal of toluene as a biomass tar surrogate in a catalytic nonthermal plasma process. Energy Fuel 2018;32:10709–19. https://doi.org/10.1021/acs.energyfuels.8b02444.
[9] Ashok J, Kawi S. Low-temperature biomass tar model reforming over perovskite materials with DBD plasma: Role of surface oxygen mobility. Energ Conver Manage 2021;248:114802. https://doi.org/10.1016/j.enconman.2021.114802.
[10] Feng D, Shang Q, Dong H, Zhang Y, Wang Z, Li D, et al. Catalytic mechanism of Na on coal pyrolysis-derived carbon black formation: Experiment and DFT simulation. Fuel Process Technol 2021;224:107011. https://doi.org/10.1016/j.fuproc.2021.107011.
[11] Cortazar M, Santamaria L, Lopez G, Alvarez J, Zhang L, Wang R, et al. A comprehensive review of primary strategies for tar removal in biomass gasification. Energ Conver Manage 2023;276:116496. https://doi.org/10.1016/j.enconman.2022.116496.
[12] Shafizadeh A, Shahbeik H, Nadian MH, Gupta VK, Nizami A-S, Lam SS, et al. Turning hazardous volatile matter compounds into fuel by catalytic steam reforming: An evolutionary machine learning approach. J Clean Prod 2023;413:137329. https://doi.org/10.1016/j.jclepro.2023.137329.
[13] Artetxe M, Alvarez J, Nahil MA, Olazar M, Williams PT. Steam reforming of different biomass tar model compounds over Ni/Al2O3 catalysts. Energ Conver Manage 2017;136:119–26. https://doi.org/10.1016/j.enconman.2016.12.092.
[14] Tang W, Cao J, Yang F, Feng X, Ren J, Wang J, et al. Highly active and stable HF acid modified HZSM-5 supported Ni catalysts for steam reforming of toluene and biomass pyrolysis tar. Energ Conver Manage 2020;212:112799. https://doi.org/10.1016/j.enconman.2020.112799.
[15] Wang Y, Yang H, Tu X. Plasma reforming of naphthalene as a tar model compound of biomass gasification. Energ Conver Manage 2019;187:593–604. https://doi.org/10.1016/j.enconman.2019.02.075.
[16] Tan R, Abdullah TAT, Jalil AA, Isa KM. Optimization of hydrogen production from steam reforming of biomass tar over Ni/dolomite/La2O3 catalysts. J Energy Inst 2020;93:1177–86. https://doi.org/10.1016/j.joei.2019.11.001.
[17] Al-Rahbi AS, Williams PT. Decomposition of biomass gasification tar model compounds over waste tire pyrolysis char. Waste Disposal & Sustainable Energy 2022;4:75–89. https://doi.org/10.1007/s42768-022-00103-5.
[18] Quan C, Wang H, Gao N. Development of activated biochar supported Ni catalyst for enhancing toluene steam reforming. Int J Energy Res 2020;44:5749–64. https://doi.org/10.1002/er.5335.
[19] Zhang H, Zhu F, Li X, Xu R, Li L, Yan J, et al. Steam reforming of toluene and naphthalene as tar surrogate in a gliding arc discharge reactor. J Hazard Mater 2019;369:244–53. https://doi.org/10.1016/j.jhazmat.2019.01.085.
[20] Xu B, Xie J, Wang N, Huang Y, Liu H, Yin X, et al. Plasma-enabled catalytic steam reforming of toluene as a biomass tar surrogate: Understanding the synergistic effect of plasma catalysis. Chem Eng J 2023;464:142696. https://doi.org/10.1016/j.cej.2023.142696.
[21] He L, Hu S, Yin X, Xu J, Han H, Li H, et al. Promoting effects of Fe-Ni alloy on co-production of H-2 and carbon nanotubes during steam reforming of biomass tar over Ni-Fe/alpha-Al2O3. Fuel 2020;276. https://doi.org/10.1016/j.fuel.2020.118116.
[22] Ren J, Cao J, Zhao X, Liu Y. Recent progress and perspectives of catalyst design and downstream integration in biomass tar reforming. Chem Eng J 2022;429:132316. https://doi.org/10.1016/j.cej.2021.132316.
[23] Zhu T, Chen Z, Gong H, Yu H, Ning P, Zhou S, et al. Seeded-growth preparation of high-performance Ni/MgAl(2)O(4)catalysts for tar steam reforming. New J Chem 2020;44:13692–700. https://doi.org/10.1039/d0nj01468k.
[24] Srinakruang J, Sato K, Vitidsant T, Fujimoto K. A highly efficient catalyst for tar gasification with steam. Catal Commun 2005;6:437–40. https://doi.org/10.1016/j.catcom.2005.03.014.
[25] Lu M, Xiong Z, Li J, Li Xi, Fang K, Li T. Catalytic steam reforming of toluene as model tar compound using Ni/coal fly ash catalyst. Asia Pac J Chem Eng 2020;15(6). https://doi.org/10.1002/apj.2529.
[26] Lu M, Xiong Z, Fang K, Li X, Li J, Li T. Steam reforming of toluene over nickel catalysts supported on coal gangue ash. Renew Energ 2020;160:385–95. https://doi.org/10.1016/j.renene.2020.06.012.
[27] Miyazawa T, Kimura T, Nishikawa J, Kado S, Kunimori K, Tomishige K. Catalytic performance of supported Ni catalysts in partial oxidation and steam reforming of tar derived from the pyrolysis of wood biomass. Catal Today 2006;115:254–62. https://doi.org/10.1016/j.cattod.2006.02.055.
[28] Lu M, Xiong Z, Fang K, Li J, Li X, Li T. Effect of promoters on steam reforming of toluene over a Ni-based catalyst supported on coal gangue ash. ACS Omega 2020;5:26335–46. https://doi.org/10.1021/acsomega.0c01197.
[29] Quitete CPB, Souza MMVM. Application of Brazilian dolomites and mixed oxides as catalysts in tar removal system. Appl Catal A 2017;536:1–8. https://doi.org/10.1016/j.apcata.2017.02.014.
[30] Lamacz A, Babinski P, Labojko G. The impact of components of synthesis gas from coal gasification on conversion of model tar compounds over Ni/CeZrO2 catalyst. Fuel 2019;236:984–92. https://doi.org/10.1016/j.fuel.2018.09.075.
[31] Quitete CPB, Bittencourt RCP, Souza MMVM. Steam reforming of tar model compounds over nickel catalysts supported on barium hexaaluminate. Catal Lett 2014;145:541–8. https://doi.org/10.1007/s10562-014-1405-3.
[32] Ahmed T, Xiu S, Wang L, Shahbazi A. Investigation of Ni/Fe/Mg zeolite-supported catalysts in steam reforming of tar using simulated-toluene as model compound. Fuel 2018;211:566–71. https://doi.org/10.1016/j.fuel.2017.09.051.
[33] Li C, Hirabayashi D, Suzuki K. Development of new nickel based catalyst for biomass tar steam reforming producing H2-rich syngas. Fuel Process Technol 2009;90:790–6. https://doi.org/10.1016/j.fuproc.2009.02.007.
[34] Ashok J, Kawi S. Nickel-iron alloy supported over iron-alumina catalysts for steam reforming of biomass tar model compound. ACS Catal 2014;4:289–301. https://doi.org/10.1021/cs400621p.
[35] Wang S, Shi Z, Jin Y, Zaini IN, Li Y, Tang C, et al. A machine learning model to predict the pyrolytic kinetics of different types of feedstocks. Energ Conver Manage 2022;260:115613. https://doi.org/10.1016/j.enconman.2022.115613.
[36] Li H, Chen J, Zhang W, Zhan H, He C, Yang Z, et al. Machine-learning-aided thermochemical treatment of biomass: a review. Biofuel Res J 2023;10:1786–809. https://doi.org/10.18331/brj2023.10.1.4.
[37] Jeon PR, Moon J-H, Ogunsola NO, Lee SH, Ling JLJ, You S, et al. Recent advances and future prospects of thermochemical biofuel conversion processes with machine learning. Chem Eng J 2023;471:144503. https://doi.org/10.1016/j.cej.2023.144503.
[38] Tang Q, Chen Y, Yang H, Liu M, Xiao H, Wang S, et al. Machine learning prediction of pyrolytic gas yield and compositions with feature reduction methods: Effects of

pyrolysis conditions and biomass characteristics. Bioresource Technol 2021;339:125581. https://doi.org/10.1016/j.biortech.2021.125581.
[39] Leng L, Zhang W, Chen Q, Zhou J, Peng H, Zhan H, et al. Machine learning prediction of nitrogen heterocycles in bio-oil produced from hydrothermal liquefaction of biomass. Bioresour Technol 2022;362:127791. https://doi.org/10.1016/j.biortech.2022.127791.
[40] Smith A, Keane A, Dumesic JA, Huber GW, Zavala VM. A machine learning framework for the analysis and prediction of catalytic activity from experimental data. Appl Catal B 2020;263:118257. https://doi.org/10.1016/j.apcatb.2019.118257.
[41] Shafizadeh A, Shahbeik H, Rafiee S, Fardi Z, Karimi K, Peng W, et al. Machine learning-enabled analysis of product distribution and composition in biomass-coal co-pyrolysis. Fuel 2024;355:129464. https://doi.org/10.1016/j.fuel.2023.129464.
[42] Yahya HSM, Abbas T, Amin NAS. Optimization of hydrogen production via toluene steam reforming over Ni-Co supported modified-activated carbon using ANN coupled GA and RSM. Int J Hydrogen Energy 2021;46:24632–51. https://doi.org/10.1016/j.ijhydene.2020.05.033.
[43] Fawcett T. An introduction to ROC analysis. Pattern Recogn Lett 2006;27:861–74. https://doi.org/10.1016/j.patrec.2005.10.010.
[44] Majnik M, Bosnić Z. ROC analysis of classifiers in machine learning: A survey. Intell Data Anal 2013;17:531–58. https://doi.org/10.3233/ida-130592.
[45] Xu H, Shen Z, Chen G, Yin C, Liu Y, Ge Z, et al. Carbon-coated mesoporous silica-supported Ni nanocomposite catalyst for efficient hydrogen production via steam reforming of toluene. Fuel 2020;275:118036. https://doi.org/10.1016/j.fuel.2020.118036.
[46] Gao N, Salisu J, Quan C, Williams P. Modified nickel-based catalysts for improved steam reforming of biomass tar: A critical review. Renew Sustain Energy Rev 2021;145:111023. https://doi.org/10.1016/j.rser.2021.111023.
[47] Oh G, Park SY, Seo MW, Kim YK, Ra HW, Lee J-G, et al. Ni/Ru–Mn/Al2O3 catalysts for steam reforming of toluene as model biomass tar. Renew Energ 2016;86:841–7. https://doi.org/10.1016/j.renene.2015.09.013.
[48] Khalifa O, Xu M, Zhang R, Iqbal T, Li M, Lu Q. Steam reforming of toluene as a tar model compound with modified nickel-based catalyst. Front Energy 2022;16(3):492–501. https://doi.org/10.1007/s11708-021-0721-8.
[49] Chen J, Sun J, Wang Y. Catalysts for steam reforming of bio-oil: a review. Ind Eng Chem Res 2017;56:4627–37. https://doi.org/10.1021/acs.iecr.7b00600.
[50] Zhou F, Pan N, Chen H, Xu X, Wang C, Du Y, et al. Hydrogen production through steam reforming of toluene over Ce, Zr or Fe promoted Ni-Mg-Al hydrotalcite-derived catalysts at low temperature. Energ Conver Manage 2019;196:677–87. https://doi.org/10.1016/j.enconman.2019.06.047.
[51] Zhang Z, Ou Z, Qin C, Ran J, Wu C. Roles of alkali/alkaline earth metals in steam reforming of biomass tar for hydrogen production over perovskite supported Ni catalysts. Fuel 2019;257:116032. https://doi.org/10.1016/j.fuel.2019.116032.
[52] Wu W, Fan Q, Yi B, Liu B, Jiang R. Catalytic characteristics of a Ni-MgO/HZSM-5 catalyst for steam reforming of toluene. RSC Adv 2020;10:20872–81. https://doi.org/10.1039/d0ra02403a.
[53] Zhang R, Wang H, Hou X. Catalytic reforming of toluene as tar model compound: Effect of Ce and Ce–Mg promoter using Ni/olivine catalyst. Chemosphere 2014;97:40–6. https://doi.org/10.1016/j.chemosphere.2013.10.087.
[54] Guo Y, He X, Su Y, Dai Y, Xie M, Yang S, et al. Machine-learning-guided discovery and optimization of additives in preparing Cu catalysts for CO2 reduction. J Am Chem Soc 2021;143:5755–62. https://doi.org/10.1021/jacs.1c00339.
[55] Jang J, Oh G, Ra HW, Yoon SM, Mun TY, Seo MW, et al. Steam reforming of toluene over Ni/coal ash catalysts: effect of coal ash composition. Korean Chem Eng Res 2021;59:232–8. https://doi.org/10.9713/kcer.2021.59.2.232.
[56] He L, Liao G, Li H, Ren Q, Hu S, Han H, et al. Evolution characteristics of different types of coke deposition during catalytic removal of biomass tar. J Energy Inst 2020;93:2497–504. https://doi.org/10.1016/j.joei.2020.08.009.
[57] Betchaku M, Nakagawa Y, Tamura M, Yabushita M, Miura Y, Iida S, et al. Catalytic performance of hydrotalcite-like-compound-derived Ni-metal alloy catalyst for toluene reforming with gasoline engine exhaust model gas as reforming agent. Fuel Process Technol 2021;218:106837. https://doi.org/10.1016/j.fuproc.2021.106837.
[58] Wang X, Su X, Zhang Q, Hu H. Effect of additives on Ni-based catalysts for hydrogen-enriched production from steam reforming of biomass. Energ Technol 2020;8. https://doi.org/10.1002/ente.202000136.